

# First measurement of the $^{10}\text{B}(\alpha, n)^{13}\text{N}$ reaction in an inertial confinement fusion implosion at the National Ignition Facility

D. Lonardonì,<sup>1, a)</sup> J. P. Sauppe,<sup>1</sup> B. D. Keenan,<sup>1</sup> M. E. Gooden,<sup>1</sup> C. B. Yeaman,<sup>2</sup> C. Velsko,<sup>2</sup> T. Murphy,<sup>1</sup> L. Kot,<sup>1</sup> T. Bredeweg,<sup>1</sup> S. H. Batha,<sup>1</sup> A. C. Hayes,<sup>1</sup> G. Jungman,<sup>1</sup> K. D. Meaney,<sup>1</sup> J. B. Wilhelmy,<sup>1</sup> and H. Huang<sup>3</sup>

<sup>1)</sup>Los Alamos National Laboratory, Los Alamos, New Mexico 87545, USA

<sup>2)</sup>Lawrence Livermore National Laboratory, Livermore, California 94550, USA

<sup>3)</sup>General Atomics, San Diego, California 92121, USA

We report the first measurement of the  $^{10}\text{B}(\alpha, n)^{13}\text{N}$  reaction in a polar-direct-drive exploding pusher (PDXP) at the National Ignition Facility (NIF). The target is composed of a 65/35 atomic % deuterium-tritium fill surrounded by a roughly  $30\mu\text{m}$  thick Beryllium ablator. The inner portion of the Beryllium ablator is doped with 10 atomic % of 10-Boron. Radiation-hydrodynamics calculations were performed in 1D to optimize both the remaining Boron rho-R and the DT neutron yield. A charged-particle transport post-processor has been developed to study  $\alpha$ -induced reactions on the ablator material. Results indicate a large 13-Nitrogen production from  $\alpha$ -induced reactions on 10-Boron, measurable by the Radiochemical Analysis of Gaseous Samples (RAGS) system at the NIF. The PDXP target N201115-001-999 was successfully fielded on the NIF, and Nitrogen from the  $^{10}\text{B}(\alpha, n)^{13}\text{N}$  reaction was measured. The  $^{13}\text{N}$  production yield, as well as the DT neutron yield, were however lower than expected, likely due to the asymmetry of the implosion.

## I. INTRODUCTION

Inertial confinement fusion (ICF)<sup>1</sup> involves a target capsule filled (usually) with DT fuel that is compressed and heated by the energy delivered to the outer ablator layer of the target using either direct laser light<sup>2</sup>, or X-rays generated inside a hohlraum illuminated by lasers<sup>3</sup>. Much of the outer layer ablates off, causing the remaining target to implode via the rocket effect. The central fuel is compressed and heated as the remaining ablator material moves inwards, and the ablator's kinetic energy is converted into fuel internal energy. As pressure builds in the DT gas, the ablator begins decelerating and eventually stagnates, representing the point at which  $PdV$  work ceases to increase the fuel energy.

During the deceleration phase of the implosion, Rayleigh-Taylor<sup>4,5</sup> (RT) instabilities can form, leading to mixing between the ablator material and the DT fuel<sup>6</sup>. The shock waves involved in the implosion can induce Richtmyer-Meshkov<sup>7,8</sup> (RM) instabilities, possibly contributing to mixing as well<sup>9</sup>. RT, RM, and other instabilities are seeded by surface finish imperfections, illumination nonuniformity, the fill tube, glue spot, and the hohlraum "tent"<sup>10-15</sup>. Mixing between the ablator material and the DT gas is undesirable, because it reduces the fuel temperature. It also raises the adiabat of the fuel<sup>16,17</sup>, making it harder to compress. Both of these effects reduce the performance of the capsule.

One method for diagnosing the mix of ablator material into the DT fuel is to study the degree of elevated X-ray emission from the burning DT fuel<sup>18</sup>. X-ray imaging can also show distortions during the implosion and the hot spot at peak compression<sup>19</sup>. However, there are capsule designs being developed for the National Ignition Facility (NIF)<sup>20</sup>, such as double shell and pushered single shell<sup>21,22</sup>, for which this X-ray technique cannot be used effectively because the designs

involve a high-Z shell surrounding the DT fuel that is opaque to X-rays.

A possible alternative mix diagnostic involves measuring the interaction of alpha particles, produced in the  $\text{D} + \text{T} \rightarrow \alpha (3.5\text{MeV}) + n (14.1\text{MeV})$  reaction, with the ablator material<sup>23</sup>. The Radiochemical Analysis of Gaseous Samples (RAGS) facility<sup>24</sup> at NIF, which collects the gaseous debris emitted into the chamber from imploded capsules, allows for quantitative measurements of  $\alpha$ -induced reactions, as long as the reaction products are gaseous. If mixing occurs, the DT  $\alpha$  production is reduced due to the decrease of the capsule performance. The reduction in DT yield from mixing may be partially compensated for by the closer proximity of the ablator materials to the alpha production region. The net effect is expected to be an overall enhancement of the  $\alpha$ -induced reactions yield in the case of mixing, making radiochemistry (RadChem) a valuable mix diagnostic for ICF studies<sup>23</sup>.

In this work, we present the first measurement of the  $^{10}\text{B}(\alpha, n)^{13}\text{N}$  reaction in an ICF implosion, using a polar-direct-drive exploding pusher (PDXP) shot at NIF, N201115-001-999, as a first step in the development of RadChem mix diagnostics. The cross-section for this reaction is shown in Fig. 1 (red circles), as discussed in Ref. 25. There is a significant peak in the cross-section for  $\alpha$  particles with  $\sim 3\text{MeV}$  of energy, slightly below the expected energy for  $\alpha$ 's produced from the D+T fusion reaction.

The N201115-001-999 target consisted of a 65/35 atomic % deuterium-tritium fill (8 atm at room temperature) surrounded by a Boron-doped Beryllium ablator. In addition to the  $^{13}\text{N}$  measurement, RAGS was also used to measure the neutron-induced reaction on Argon  $^{40}\text{Ar}(n, \gamma)^{41}\text{Ar}$ , providing an additional diagnostic for the areal density of the remaining ablator material at the time of the DT burn, in a similar manner as Ref. 26. (Argon was present in the Beryllium ablator as a by-product of the sputter-coating fabrication process.) The gamma reaction history (GRH) capability<sup>27</sup> was used to measure 4.4 MeV gamma from the de-excitation of Carbon  $2^+$  excited states coming from the  $^9\text{Be}(\alpha, n)^{12}\text{C}^*$  reaction, as

<sup>a)</sup>Electronic mail: lonardonì@lanl.gov

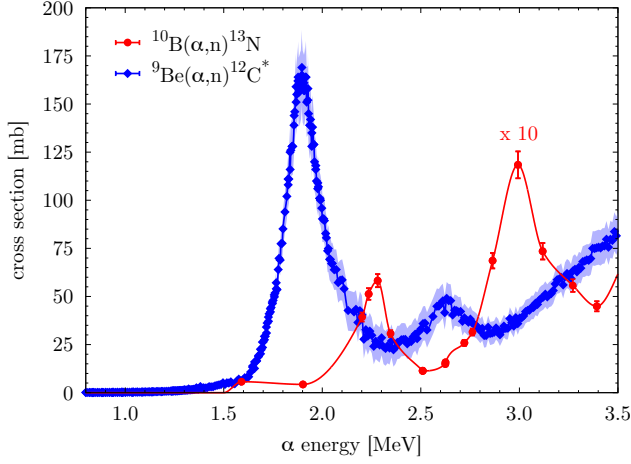


Figure 1. Experimental cross sections as a function of the incident  $\alpha$ -particle energy (laboratory reference frame). Red dots and error bars for  $^{10}\text{B}(\alpha, n)^{13}\text{N}$  (ground-state transition) from Liu *et al.*<sup>25</sup>. Blue diamonds and error bands for  $^9\text{Be}(\alpha, n)^{12}\text{C}^*$  ( $\gamma$  @ 4.4 MeV) from the EXFOR database<sup>28</sup>. Solid lines are interpolations on the experimental results.

a cross calibration for the RadChem diagnostic. This cross-section is also shown in Fig. 1 (blue diamonds). The capsule produced  $4.04 \cdot 10^{14}$  DT neutrons, and approximately  $7 \cdot 10^6$  13-Nitrogen and  $10^5$  41-Argon. A combination of low signal and competition between the 4.4 MeV and the DT fusion gamma rays allowed only an upper limit of  $2 \cdot 10^{12}$  of the 4.4 MeV gamma ray yield, see Table I.

This manuscript is organized as follows. In Section II, we discuss the target design and fabrication process. We introduce the 1D pre-shot modeling and the RadChem post-processing framework in Section III, and discuss sensitivities observed from applying this methodology to our 1D simulations. The experimental results are presented in Section IV, and more detailed 2D post-shot modeling is also considered here. Lastly, we conclude in Section V and discuss next steps for the platform.

Table I. Summary of the experimental results for the N201115-001-999 PDXP shot. The last column reports the source/detector used for the estimates.

$^{10}\text{B}$ dopant level	$\sim 10$ atomic %	GA estimate
$^{40}\text{Ar}$ concentration	$\sim 0.3$ atomic %	GA estimate
Bang time	$4.5 \pm 0.5$ ns	GRH <sup>27</sup>
	$4.83 \pm 0.13$ ns	SPIDER <sup>29</sup>
Burn width	$600 \pm 75$ ps	GRH
	$618.50 \pm 270.59$ ps	SPIDER
DTn yield	$4.040 \pm 0.126 \cdot 10^{14}$	nTOF <sup>30</sup>
$^{13}\text{N}$ yield	$\sim 7 \cdot 10^6$	RAGS <sup>24</sup>
$^{41}\text{Ar}$ yield	$\sim 1 \cdot 10^5$	RAGS
$\gamma$ (4.4 MeV) yield	$< 2 \cdot 10^{12}$	GRH

## II. TARGET DESIGN AND FABRICATION

We based our original design on a previously developed low-convergence, high-yield polar direct-drive exploding pusher platform<sup>31</sup>. The particular capsule we chose to emulate was fielded on NIF shot N190707-001-999 (colloquially known as “Little Guy”), a CH ablator target that yielded  $4.8 \times 10^{15}$  neutrons<sup>32</sup>. In that design, the laser drive was optimized to minimize multi-dimensional effects, enabling physics studies in an approximately 1D configuration. Further, this laser drive has the advantage of inducing no known optics damage at NIF, providing a robust neutron signal with no risk to the laser. In this design work, we opted to keep the same laser pulse history and beam pointings due to the record performance achieved.

In order to measure the primary  $^{10}\text{B}(\alpha, n)^{13}\text{N}$  reaction, the capsule design had to be modified to include  $^{10}\text{B}$  near the DT fuel region, placing it in close proximity to the  $\alpha$  particles produced from thermonuclear burn. However, it proved difficult to fabricate leak-tight pure Boron ablators that can hold DT gas at the required fill pressures, limiting our design choices to only utilizing a doped  $^{10}\text{B}$  region. In a CH ablator, 13-Nitrogen can also be produced from the competing reactions  $^{12}\text{C}(d, n)^{13}\text{N}$  and  $^{13}\text{C}(p, n)^{13}\text{N}$ . This background production from Carbon can potentially be comparable to the production from Boron<sup>25</sup>, posing significant technical challenges to the extraction of the  $\alpha$ -induced contribution from the total signal. Instead, we considered a Beryllium ablator layer with a region of Boron-doped Beryllium on the inner part of the capsule. This has the additional advantage of providing a complementary diagnostic via the measurement of 4.4 MeV gammas coming from the  $^9\text{Be}(\alpha, n)^{12}\text{C}^*$  ( $\gamma$  @ 4.4 MeV) reaction.

We note that the relevant reactions for this study are only those populating the 13-Nitrogen lowest-energy state, the angle-integrated cross section of which has been recently re-measured in the energy range relevant for DT nuclear burn<sup>25</sup> (see Fig. 1). In fact, the ground-state of  $^{13}\text{N}$  has a half-life of  $t_{1/2} = 9.965(4)$  min<sup>33</sup>, long enough to allow collection using RAGS.  $^{13}\text{N}$  excited states are proton unbound and will, instead, immediately decay to stable  $^{12}\text{C}$ .

The long half-life of  $^{41}\text{Ar}$  ( $t_{1/2} = 109.61(4)$  min<sup>34</sup>) makes it a good candidate for collection at RAGS, allowing us to also measure the reaction  $^{40}\text{Ar}(n, \gamma)^{41}\text{Ar}$ . The sputter-coating process used to fabricate these capsules results in a small amount of Argon being uniformly deposited within the ablator as well. From our analysis of the fabricated capsule, the  $^{40}\text{Ar}$  concentration in the ablator shell was estimated to be of the order of 0.3 atomic %. Indirect-drive targets are sensitive to the Argon concentration, primarily as a result of the modification in the opacity of the ablator<sup>26</sup>. However, this is not as well studied for direct-drive targets. Preliminary modeling, discussed in Section III C, finds sensitivity to the Argon concentration.

During the fabrication process of the target, we conducted three different coating runs to test the addition of  $^{10}\text{B}$  dopant to a Beryllium ablator. The first run resulted in a leak-tight capsule with good surface quality. However, the amount of Boron introduced in the ablator was estimated to be much less than anticipated, of the order of  $\sim 5$  atomic %. With

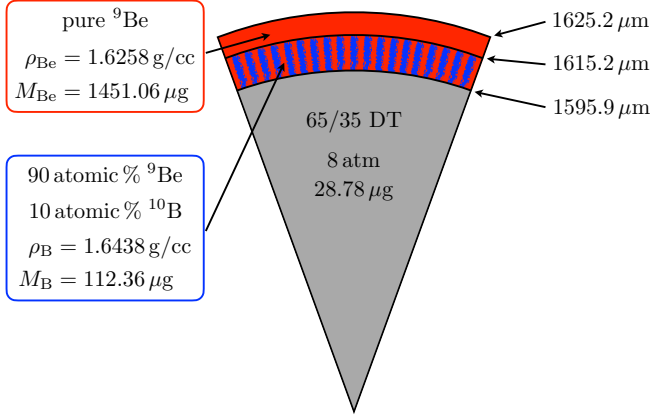


Figure 2. Details of the PDXP target used in 1D xRAGE calculations. The composite density of the ablator doped layer is computed as  $\rho_{\text{total}} = (f_{\text{Be}} + 9/10 f_{\text{B}}) \rho_{\text{Be}}$ , where  $f_X$  is the atomic fraction of the species X. The ablator also contains a 0.3 atomic % of  $^{40}\text{Ar}$ .

the second run, the  $^{10}\text{B}$  dopant level reached  $\sim 20$  atomic %, but the target was not leak-tight. The third and final run produced a leak-tight capsule with an intermediate value of  $\sim 10$  atomic % of  $^{10}\text{B}$  dopant. However, the Beryllium ablator did not shrink as much as expected during pyrolysis of the target mandrel, and the outer radius was much larger than originally designed. The resulting capsule had an inner radius of  $\sim 1600 \mu\text{m}$ , and it was filled with 65/35 atomic % DT at 8 atm, for a total fuel mass of  $28.78 \mu\text{g}$  (Fig. 2). There is a  $\sim 19 \mu\text{m}$  thick 10 atomic % Boron-doped Beryllium layer surrounded by a  $10 \mu\text{m}$  pure Beryllium layer. With this configuration, the total mass of the Boron dopant is  $112.36 \mu\text{g}$ , and the average density of the ablator was estimated at  $1.64 \text{ g/cc}$ .

### III. PRE-SHOT ANALYSIS

#### A. Computational Modeling

We initially carried out a series of pre-shot design simulations using xRAGE<sup>11,35</sup>, the Los Alamos National Laboratory's Eulerian radiation-hydrodynamics code. A laser package has recently been implemented for 1D and 2D xRAGE computations.<sup>36,37</sup> Here, we use an *ad hoc* laser power multiplier,  $\eta_{\text{laser}}$ , to reduce the input laser energy to account for cross-beam energy transfer (CBET) or other laser plasma instabilities (LPI) that are not currently modeled. Often, radiation-hydrodynamics codes utilize a Spitzer-Harm thermal conduction with a flux limiter  $f_e$  that is used to limit the rate at which heat can be transported (for more details see Ref. 38 and references therein). We first modeled the CH capsule N190707 using 1D xRAGE simulations in order to calibrate  $\eta_{\text{laser}}$  and  $f_e$ , following Ellison *et al.*<sup>31</sup>. We performed a two-dimensional scan of the parameter space, seeking to match the observed DT yield and the bang time as closely as possible. The best match to N190707 was found for  $\eta_{\text{laser}} = 0.65$  and  $f_e = 0.05$ .

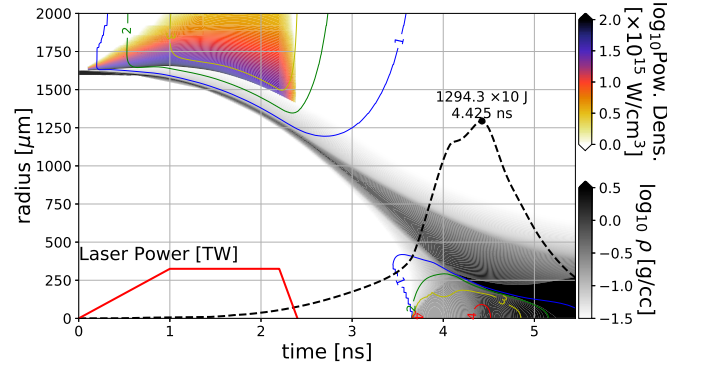


Figure 3.  $r-t$  contour plot of the implosion of the N20115 target. Log density (grayscale), laser power deposition (color), and temperature (colored lines, in keV) from 1D xRAGE computations.

Having calibrated our 1D simulations to match the existing data from N190707, we then performed our preliminary design simulations for the N201115 target. However, in subsequent post-shot modeling, we found that we could get a better match to the observed bang time (see Table I) in these flux-limited calculations using a higher laser power multiplier,  $\eta_{\text{laser}} = 0.85$ . This likely points to key differences in the ablation efficiencies of CH and Be. Similar behavior has been observed in HYDRA<sup>39</sup> calculations, where a larger power multiplier is needed for Be ablators relative to CH ablators<sup>40</sup>. All the results presented in the next sections have been obtained using  $\eta_{\text{laser}} = 0.85$  and  $f_e = 0.05$  in 1D xRAGE calculations.

In our modeling of N201115, the  $^{10}\text{B}$  and  $^9\text{Be}$  are included as separate materials, each with their respective equations of state (EOS) from the Livermore Equations of State (LEOS) database<sup>41</sup> and opacities as calculated from the OPLIB database<sup>42</sup> using the TOPS code<sup>43</sup>. The materials are premixed in the appropriate atomic fractions in the doped region of the ablator. The inclusion of a small fraction of  $^{40}\text{Ar}$  into the  $^{10}\text{B}$  and  $^9\text{Be}$  materials in our computations has been carried out by modifying the opacities for both materials. We also modified the isotopic concentrations to include the Argon component, as isotopics are important for the 3T package which impacts the laser deposition. However, the equations of state were left unchanged in this study.

The dynamics of the implosion are best illustrated in the  $r-t$  contour plot from a 1D xRAGE simulation, shown in Fig. 3. The density contours are shown in grayscale and the laser power deposition is illustrated in the color contours. The laser drive lasts for the first 2.4 ns of the implosion, ablating material off of the outer surface of the capsule and driving the remaining mass inwards. The shell was designed such that the inner  $^{10}\text{B}$ -doped portion would be mostly intact at stagnation, providing sufficient targets for the  $\alpha$  particles, while the outermost pure Beryllium layer was ablated off. As the shell coasts inwards, its kinetic energy is converted into internal energy of the DT fuel, which is shown in the dashed black line of Fig. 3. The peak value occurs at 4.45 ns, which can be used as a proxy for bang time.

Given the fuel conditions as a function of time, we calcu-

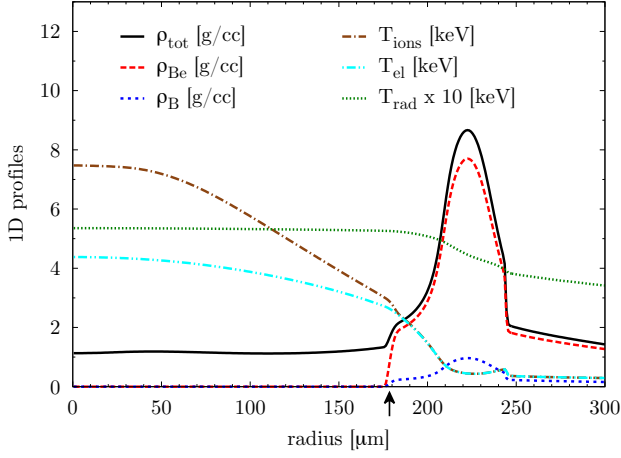


Figure 4. Density and temperature profiles from 1D xRAGE calculations corresponding to the bang time conditions of Fig. 3. The position of the fuel-ablator interface at bang time is shown with a black arrow.

lated the DT neutron production rate, resulting in a predicted total yield of  $2.60 \cdot 10^{15}$  and a burn width of 302 ps (see also Fig. 6 and Table II). The corresponding bang time density and temperature profiles (assuming no hydrodynamical mix between the fuel and the ablator shell material) are shown in Fig. 4. At this time, the fuel-ablator interface is situated at  $178.5 \mu\text{m}$ , with a DT average density of  $1.15 \text{ g/cc}$  and a peak ablator density of  $8.67 \text{ g/cc}$ . The central ion and electron temperatures are  $7.5 \text{ keV}$  and  $4.4 \text{ keV}$ , respectively. The radiation temperature in the capsule is much smaller, only about  $530 \text{ eV}$ .

## B. RadChem Analysis

We developed a charged-particle transport post-processor in order to study  $\alpha$ -induced reactions in the ablator material. Given the generic reaction  $X(\alpha, n)Y$ , the final number of nuclei  $N_Y$  is given by the integral over energy and time of the  $\alpha$ -particle flux  $\Phi_\alpha(E, t)$ , multiplied by the reaction cross-section  $\sigma_{\alpha X}(E)$  and the initial number of nuclei  $N_X$ :

$$N_Y = \int dt \int dE \Phi_\alpha(E, t) \sigma_{\alpha X}(E) N_X, \quad (1)$$

where the energy integral is evaluated for  $\alpha$ -particle energies from  $3.5$  to  $0 \text{ MeV}$ . In our study,  $X = ^{10}\text{B}$ ,  $^9\text{Be}$  and  $Y = ^{13}\text{N}$ ,  $^{12}\text{C}^*$ , respectively.

The time-dependent 1D xRAGE density and temperature profiles have been used to track the energy loss of  $\alpha$  particles produced in different regions of the fuel due to the stopping power in the target plasma (both within the DT fuel and the ablator material). The  $\alpha$  stopping power is calculated according to Zimmerman<sup>44</sup>, and includes contributions from free electrons and ions in the plasma. No bound electron contribution is considered, as the plasma is fully ionized at the temperatures considered here.

The implosion and nuclear burn conditions of N201115

Table II. Summary of the 1D xRAGE-RadChem analysis of the design shown in Fig. 2.

$^{10}\text{B}$ dopant level	10 atomic %
$^{40}\text{Ar}$ concentration	0.3 atomic %
bang time	4.450 ns
burn width	302 ps
DTn yield	$2.60 \cdot 10^{15}$
$^{13}\text{N}$ yield	$2.65 \cdot 10^8$
$^{41}\text{Ar}$ yield	$1.50 \cdot 10^7$
$\gamma$ (4.4 MeV) yield	$3.21 \cdot 10^{10}$

from 1D xRAGE computations are such that all of the  $\alpha$  particles produced into the DT fuel are predicted to reach and cross the fuel-ablator interface. They all eventually stop within the ablator, where  $\alpha$ -induced reactions on  $^{10}\text{B}$  and  $^9\text{Be}$  can occur (no mix assumed). At bang time,  $\alpha$  particles get trapped within  $\sim 44 \mu\text{m}$  into the ablator, that roughly corresponds to the position of the peak density of Boron and Beryllium (see Fig. 4).

We note that, as a result of the relative large size of the fuel region, a non-negligible fraction of  $\alpha$  particles lose a considerable amount of energy (up to  $\sim 1.5 \text{ MeV}$ ) before reaching the ablator. This greatly affects the yield of  $\alpha$ -induced reactions as the relevant cross sections are strongly energy dependent (see Fig. 1). The  $14.1 \text{ MeV}$  DT neutrons are in stark contrast to this, as they can travel almost unperturbed through the plasma (minimal energy loss), producing  $^{41}\text{Ar}$  in the ablator via the reaction  $^{40}\text{Ar}(n, \gamma)^{41}\text{Ar}$ , that has a cross section of  $\sigma(14.1 \text{ MeV}) = 0.449 \text{ mb}$ <sup>28</sup>.

A summary of the 1D xRAGE-RadChem analysis is reported in Table II. The predicted DTn yield is  $2.60 \cdot 10^{15}$ . The expected  $^{13}\text{N}$  and  $^{41}\text{Ar}$  signals are of the order of  $10^8$  and  $10^7$ , respectively. Both signals exceed the corresponding RAGS thresholds ( $10^6$  and  $10^4$ , respectively), and are thus measurable. The  $4.4 \text{ MeV}$   $\gamma$  signal from the  $^9\text{Be}(\alpha, n)^{12}\text{C}^*$  reaction is expected to be above  $10^{10}$ , value also theoretically measurable by the GRH detector.

Fig. 5 shows the  $r-t$  contour plot for the predicted particle yields achieved during the N201115 implosion, left to right for DTn,  $^{13}\text{N}$ ,  $^{41}\text{Ar}$ , and  $4.4 \text{ MeV}$   $\gamma$ . Bang time is highlighted with a white upward triangle, and the position of the fuel-ablator interface is also displayed with a white dashed curve. The latter matches the contours for DT neutrons and  $\alpha/n$ -induced reactions as no hydrodynamical mix between the fuel and the ablator material has been considered in this run. The DTn profile shows an early neutron production for  $t \lesssim 4.1 \text{ ns}$ . This corresponds to the shock yield and has minimal impact on  $\alpha/n$ -induced reactions in the ablator. During the following DT nuclear burn, the fuel region is compressed from  $\sim 275 \mu\text{m}$  to  $\sim 125 \mu\text{m}$ , with the peak neutron production at bang time localized between  $\sim 50 \mu\text{m}$  and  $\sim 125 \mu\text{m}$ .  $\alpha$ -induced reactions on  $^{10}\text{B}$  and  $^9\text{Be}$  are confined in a narrow region close to the fuel-ablator interface, as the alpha particles quickly lose energy into the ablator material and eventually



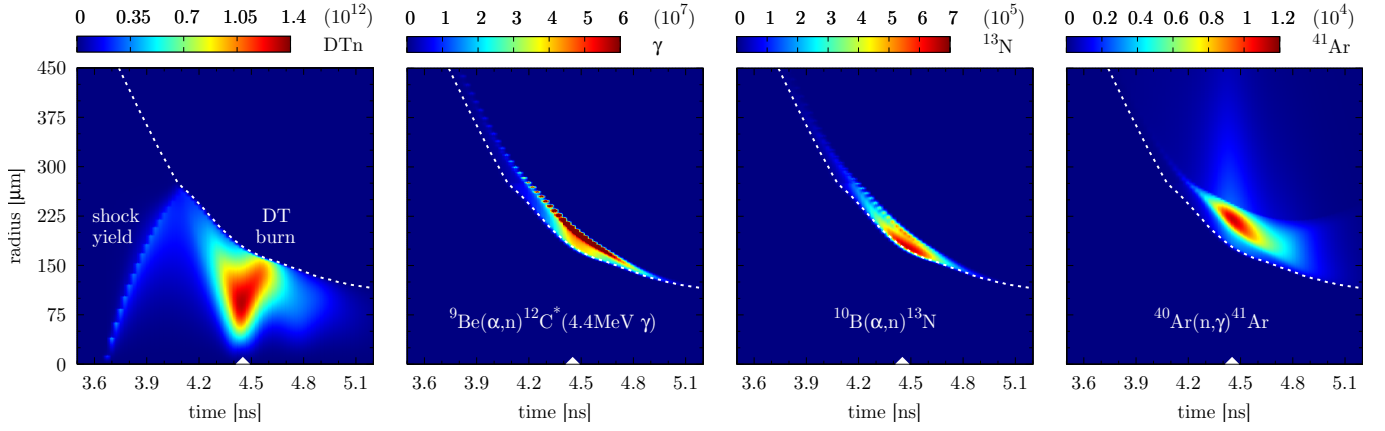


Figure 5.  $r-t$  contour plot of the implosion of the N20115 target. From left to right, particle yield for DTn,  $^{13}\text{N}$ ,  $^{41}\text{Ar}$ , and 4.4 MeV  $\gamma$  from the RadChem analysis of 1D xRAGE computations. The white dashed curve corresponds to the position of the fuel-ablator interface. The white upward triangle indicates bang time, 4.450 ns. Imperfections in the color map are due to the somewhat limited temporal resolution (25 ps) of the xRAGE outputs.

stop. The  $^{41}\text{Ar}$  production covers instead a wider spatial region as the more energetic neutrons are able to travel much farther on average before an interaction occurs.

The time-dependent (position-integrated) yields are shown in Fig. 6. The DTn shock yield is identifiable for earlier times ( $t \lesssim 4.1$  ns). As already mentioned, this earlier signal does not significantly contribute to  $\alpha/n$ -induced reactions, as also visible in this figure. Note the shoulder of  $^{41}\text{Ar}$  production for later times compared to the  $^{13}\text{N}$  and  $\gamma$  signals, consequence of the difference in alpha and neutron transport through the ablator material (see the corresponding spatial distributions at later times in Fig. 5).

### C. Sensitivity Study

The xRAGE-RadChem analysis presented so far refers to the capsule design illustrated in Fig. 2, that includes a 10 atomic %

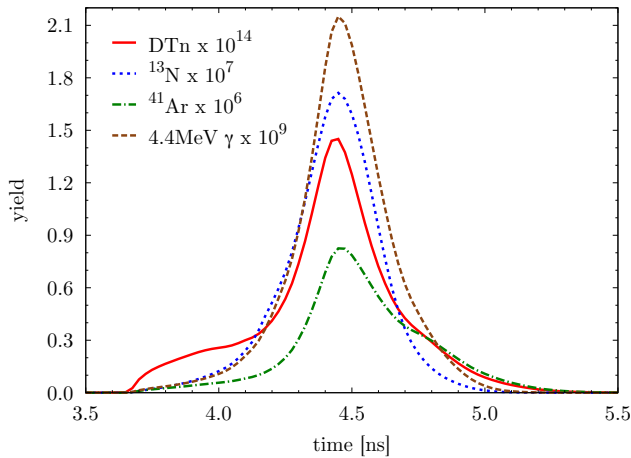


Figure 6. DTn,  $^{13}\text{N}$ ,  $^{41}\text{Ar}$ , and 4.4 MeV  $\gamma$  time-dependent yields.

$^{10}\text{B}$  dopant level and a 0.3 atomic %  $^{40}\text{Ar}$  concentration in the ablator. An accurate determination of the Boron and Argon concentrations in the manufactured N201115-001-999 capsule is however very challenging. We examined sensitivity to the  $^{10}\text{B}$  dopant level (within few percent) in our simulations, but we found little change in the simulated neutron yields and RadChem results. Changes in the Argon concentration, instead, result in larger modifications of the implosion and burn properties (see Table III).

Adding Argon results in the ablator becoming more diffuse during the coasting phase, likely an effect of the increased opacity. Essentially, the Argon acts as a sink for photons, and the ablator heats up and expands during the coasting as a result of absorption of this “extra” energy. During the laser drive phase, the peak radiation temperature in the Boron-dopant material is 100 eV without any Argon, while with 1.5 atomic %  $^{40}\text{Ar}$  the peak radiation temperature in the Boron is 120 eV. There is not a large effect on the inner surface trajectory, and the reported laser energy absorbed by the capsule is comparable in all cases. Increasing the  $^{40}\text{Ar}$  concentration results in a lower peak ablator density at stagnation, owing to the more diffuse ablator. Increasing the Argon percentage drops the DTn yield considerably and results in larger burn widths. This has a considerable impact on  $\alpha$ -induced reactions, with  $^{13}\text{N}$  and 4.4 MeV  $\gamma$  yields decreasing by roughly a factor 5 moving from no Argon to 1.5 atomic %  $^{40}\text{Ar}$  concentration.

From the above analysis, it is evident that Argon is not a passive ride-along for direct-drive implosions. It results in reduced performance, owing to a more diffuse ablator during the coasting phase. However, it is possible that the detrimental effects of Argon in the ablator might be mitigated somewhat by a shorter coast time, giving the ablator less time to decompress as a result of the absorbed radiation energy.

Table III. Summary of the 1D xRAGE-RadChem analysis for different  $^{40}\text{Ar}$  concentrations. For these runs the  $^{10}\text{B}$  dopant level has been set to 10 atomic %.

$^{40}\text{Ar}$ concentration	0 atomic %	0.3 atomic %	0.5 atomic %	1.5 atomic %
bang time	4.450 ns	4.450 ns	4.425 ns	4.425 ns
burn width	291 ps	302 ps	310 ps	380 ps
DTn yield	$3.48 \cdot 10^{15}$	$2.60 \cdot 10^{15}$	$2.31 \cdot 10^{15}$	$1.58 \cdot 10^{15}$
$^{13}\text{N}$ yield	$4.44 \cdot 10^8$	$2.65 \cdot 10^8$	$2.10 \cdot 10^8$	$9.55 \cdot 10^7$
$^{41}\text{Ar}$ yield	0	$1.50 \cdot 10^7$	$2.14 \cdot 10^7$	$3.82 \cdot 10^7$
$\gamma$ (4.4 MeV) yield	$5.54 \cdot 10^{10}$	$3.21 \cdot 10^{10}$	$2.52 \cdot 10^{10}$	$1.21 \cdot 10^{10}$

#### IV. EXPERIMENTAL RESULTS

The NIF shot N201115-001-999 produced an estimated  $\sim 4 \cdot 10^{14}$  DT neutrons, only  $\sim 16\%$  of the predicted 1D yield, with significant shape asymmetry. The capsule bang time occurred at  $4.83 \pm 0.13$  ns ( $4.5 \pm 0.5$  ns) based on the SPIDER (GRH) measurement, and the burn duration (full-width-at-half-maximum) was  $600 \pm 75$  ps according to the GRH analysis (see Table I for details).

The neutron production region was very large, with a sizeable  $P_2$  asymmetry and modest azimuthal asymmetry. A 3D reconstruction of the neutron production region for this shot is shown in Fig. 7, produced from two independent lines-of-sight utilizing the procedure described in Ref. 45. The first line-of-sight views the capsule from near the northern pole of the target chamber at  $\theta = 5^\circ$  and  $\phi = 225^\circ$ , while the second line-of-sight views the capsule from the equator looking from  $\theta = 90^\circ$  and  $\phi = 315^\circ$ . The 2D images from each diagnostic port are also shown in Fig. 7.

The dominant Fourier component from a decomposition of the polar view is  $m = 2$  with  $m_2/m_0 \sim 5.97\%$ , and there was also a significant  $m = 6$  azimuthal feature with  $m_6/m_0 \sim 3.14\%$ . The azimuthal asymmetry is here attributed to the fact that two NIF quads (sets of four beams) had to be dropped for this shot. However, these dropped beams do not explain the significantly pancaked (oblate) implosion, which was found to have very large Legendre  $P_2$  and  $P_4$  components as extracted from the equatorial view. The average ( $P_0$ ) radius of the neutron production region was estimated to be quite large,  $\sim 212 \mu\text{m}$ , with  $P_2/P_0 \sim -48.5\%$  and  $P_4/P_0 \sim 17.4\%$ . These numbers are summarized in the inset table of Fig. 7. As will be demonstrated subsequently, this shape asymmetry can be reproduced in preliminary 2D xRAGE post-shot modeling.

##### A. Radiochemical Signatures

Both  $^{13}\text{N}$  and  $^{41}\text{Ar}$  were detected at RAGS.  $^{13}\text{N}$  is collected directly into the RAGS abort tank, bypassing the getters, and assayed by measuring its  $t_{1/2} = 9.97$  min decay by positron emission. The RAGS collection efficiency of  $^{13}\text{N}$  is not fully characterized at this time. The collection efficiency has been measured for those circumstances where  $^{13}\text{N}$  is pro-

duced in a hohlraum via the  $^{13}\text{N}(n, 2n)^{14}\text{N}$  reaction, but this is not necessarily the same as the collection efficiency for direct drive shots because possible nitrogen molecular formation in the NIF chamber could depend on configuration geometry. Thus, although we saw a very clear  $^{13}\text{N}$  signal at RAGS, we were only able to estimate the number of  $^{13}\text{N}$  atoms produced at the time of capsule burn. The collection scheme for  $^{41}\text{Ar}$  at RAGS is described in Ref. 26, and it is assayed using a calibrated HPGe detector to measure the  $\gamma$ -rays emitted in  $t_{1/2} = 109.61$  min beta-decay of  $^{41}\text{Ar}$ . The measured signals for both  $^{13}\text{N}$  and  $^{41}\text{Ar}$  were considerably lower than expected based on the 1D pre-shot predictions, and at least part of this may be ascribed to the reduced DT neutron yield.

The signal for the GRH diagnostic was quite noisy, complicating the analysis. However, a crude upper limit of  $2 \cdot 10^{12}$  4.4 MeV  $\gamma$ 's was obtained. The ratio of DT fusion gammas versus  $^9\text{Be}$  induced gammas makes the 4.4 MeV  $\gamma$  measurement difficult. In the future, higher DT fusion and 4.4 MeV gamma ray yields can leverage filtering techniques to make a cleaner, more definitive measurement.

##### B. Initial Post-Shot Modeling

In order to better understand the source of the shape asymmetry, we performed a preliminary 2D post-shot computation. The as-fired laser beam configuration, including the beam pointings and elliptical beam spots, was imported into xRAGE, allowing us to capture the polar aspects of the drive though the azimuthal variation was artificially symmetrized here. In this initial computation, we used the as-designed laser pulse with all beams at nominally the same power. Further, we did not drop the missing quads here, which would require 3D computations to fully capture; a 3D laser ray-trace capability is being developed for xRAGE, but it is not yet available. Further, the experiment used wavelength detuning on some of the beams in an attempt to mitigate CBET. While a CBET package is available in xRAGE, it increases the computational cost considerably, and so this wavelength detuning is also neglected at this time. Lastly, our initial 2D simulation neglected the Argon dopant in the ablator material. All of these effects will be considered more fully in future simulations.

Results from this preliminary 2D simulation are shown in Fig. 8. The first panel shows the laser power deposition in

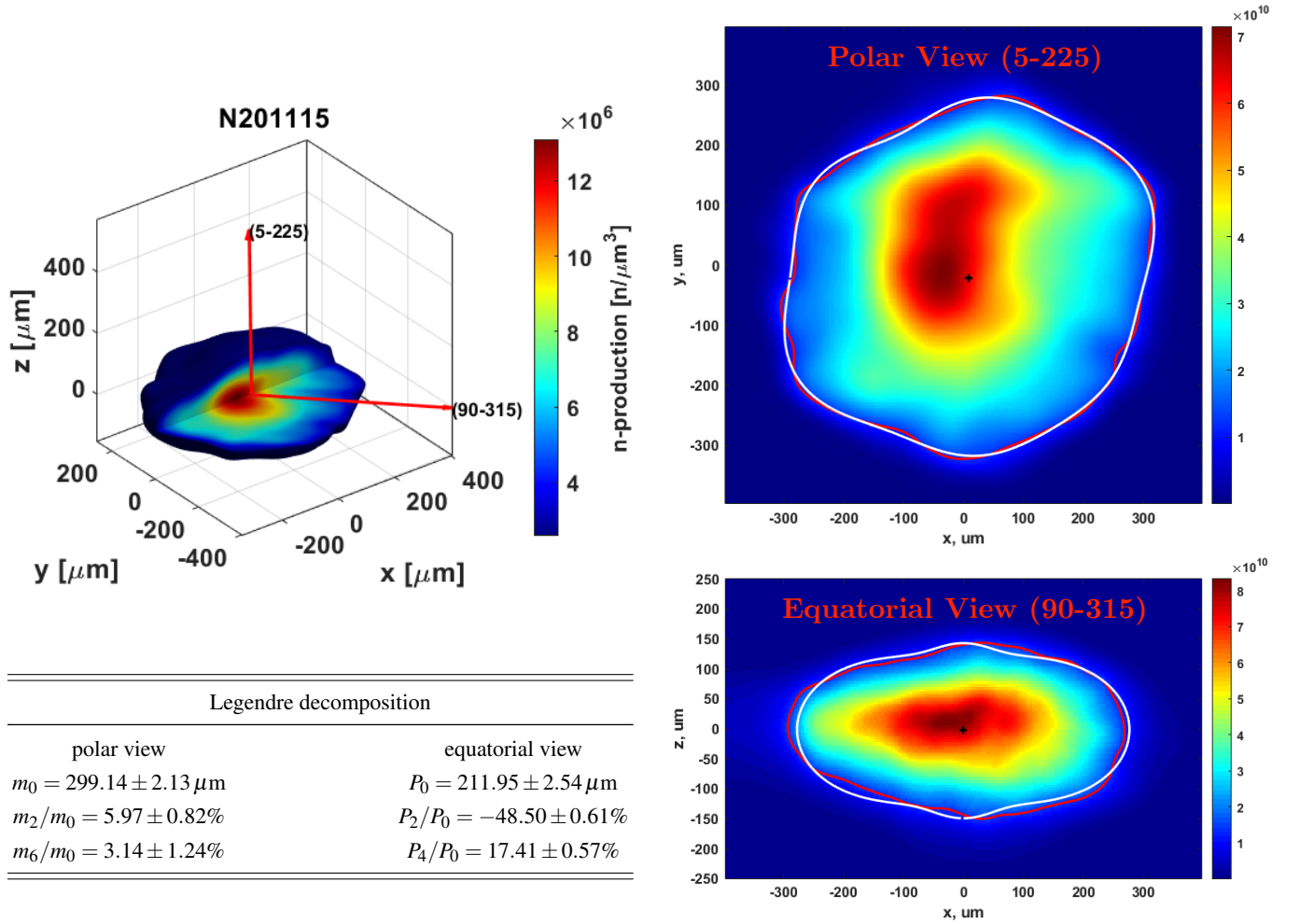


Figure 7. Reconstructed DT neutron production distribution of the N201115-001-999 PDXP shot. Top left panel: full 3D reconstruction. Right panels: polar view (top) and equatorial view (bottom). Bottom left table: dominant Fourier components from the Legendre decomposition of the polar and equatorial views. Uncertainties include both statistical and systematic errors added in quadrature.

color and the mass density in gray-scale partway through the flattop portion of the laser drive. Even at this early time, it is clear that the drive is smaller at the equator than at the poles, which is typical of polar direct-drive capsules. The next four panels show the mass density (gray-scale) and contours of the ion temperature in the colored lines (blue = 1 keV, green = 2 keV, and red = 3 keV) at several points leading up to stagnation. It is immediately clear that both the incoming unablated material and the central gas region are very oblate as a result of the polar laser drive configuration.

Bang time for this simulation occurs at 4.55 ns, which is close to the SPIDER result and consistent with the GRH estimate (see Table I). The simulated DT neutron yield is  $7.274 \cdot 10^{14}$ , roughly 28% of the predicted 1D neutron yield, but only a factor of  $\sim 1.8\times$  higher than the experimentally measured value. It is expected that the simulated yield will be further reduced when azimuthal asymmetries from the dropped quads and engineering defects, such as the capsule fill tube, are also incorporated into the simulation. These values are summarized in Table IV.

Legendre analysis of the central ion temperature contours at 4.5 ns finds significant levels of  $P_2$  and  $P_4$  asymmetry that are consistent with the experimentally observed values. The 3 keV contour has  $P_0 = 179.23 \mu\text{m}$ ,  $P_2/P_0 = -56.89\%$ , and  $P_4/P_0 = 42.12\%$ , while the 5 keV contour has  $P_0 = 115.72 \mu\text{m}$ ,  $P_2/P_0 = -59.38\%$ , and  $P_4/P_0 = 22.54\%$ . These values are also reported in Table IV. Recall that the experimentally measured values, taken from analysis of the neutron production region rather than an ion temperature contour, were  $P_0 = 211.95 \mu\text{m}$ ,  $P_2/P_0 = -48.50\%$  and  $P_4/P_0 = 17.41\%$ . Our preliminary xRAGE calculation is thus qualitatively consistent with these results, despite the missing elements noted previously. We expect that this agreement will be improved as our modeling fidelity increases.

### C. Discussion

The significant asymmetry observed in both the experimental data for N201115 and the preliminary post-shot

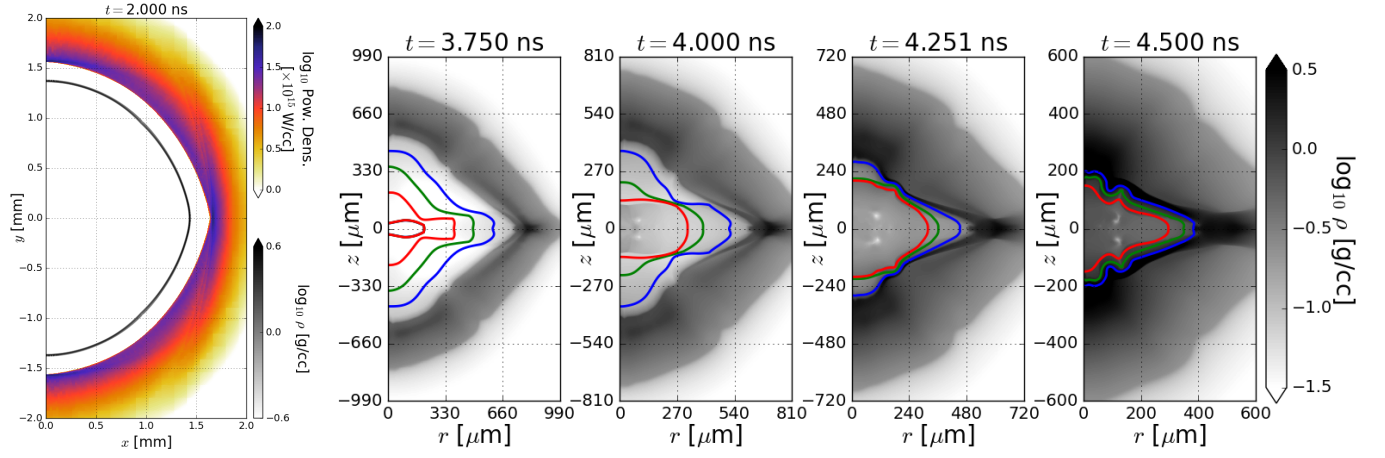


Figure 8. Leftmost image shows laser power deposition (color) and density (grayscale), while images to the right show density (grayscale) and ion temperature contours (blue = 1 keV, green = 2 keV, red = 3 keV) from a 2D xRAGE computation of N201115. The simulation predicts a very oblate implosion, in agreement with the experimentally observed hot spot shape.

Table IV. Summary of the 2D xRAGE results. The Legendre decomposition is shown for two different temperatures contours near stagnation.

$^{10}\text{B}$ dopant level	10 atomic %	
$^{40}\text{Ar}$ concentration	0 atomic %	
bang time	4.550 ns	
burn width	349 ps	
DTn yield	$7.274 \cdot 10^{14}$	
	3 keV	5 keV
Legendre	$P_0 = 179.23 \mu\text{m}$	$P_0 = 115.72 \mu\text{m}$
decomposition	$P_2/P_0 = -56.89\%$	$P_2/P_0 = -59.38\%$
	$P_4/P_0 = 42.12\%$	$P_4/P_0 = 22.54\%$

xRAGE simulations clearly demands a more sophisticated post-processing of the radiochemical signatures beyond the simple 1D model introduced previously. Work is ongoing to develop such a framework, but at this time we are unable to make any statements comparing the observed radiochemical measurements to our simulation predictions. It is also expected that hydrodynamic instabilities, which lead to mixing of the Boron/Beryllium ablator material into the DT fuel region, can alter the expected RadChem signals. Disentangling these effects is the subject of ongoing investigations.

One point worth mentioning is that, as noted previously, this capsule was quite a bit larger,  $\sim 1625 \mu\text{m}$  outer radius, than the original design dimensions based on N190707-001, which was only  $\sim 1480 \mu\text{m}$  outer radius. We did not attempt to alter the beam pointings to account for the larger radius capsule of N201115-001, so this likely accounts for at least some of the asymmetry observed here. However, it should be noted that N190707-001 also had a somewhat oblate neutron emission region<sup>32</sup>, although the performance was considerably greater ( $4.81 \cdot 10^{15}$  DT neutrons). In order to get an

estimate of how much the larger radius capsule changed the shape, we ran a preliminary 2D xRAGE simulation of N190707 using a lower laser power multiplier of  $\eta_{\text{laser}} = 0.65$  to approximately match bang time for this CH ablator capsule. However, we still neglected CBET and the wavelength detuning in this first-pass analysis. We found that even the smaller radius of N190707 still produced a fairly oblate implosion in xRAGE. That is, even had the Boron/Beryllium ablator capsule been the correct radius, we would likely still have observed an oblate implosion with reduced performance. Clearly, additional work is needed to improve the drive conditions for these polar-drive targets.

## V. CONCLUSIONS

The goal of the current experiment was to test the feasibility of producing  $^{13}\text{N}$  through the  $^{10}\text{B}(\alpha, n)^{13}\text{N}$  reaction in a PDXP at the NIF. This was motivated by the need to develop an alpha-particle induced RadChem mix diagnostic for more complicated inertial confinement fusion capsule designs. We observed a very robust  $^{13}\text{N}$  signal using the RAGS facility at NIF, despite the fact that our PDXP yield was quite suppressed compared to 1D clean estimates. The low DT yield resulted mainly from the very asymmetric implosion achieved, which in turn resulted from the fact that the laser beam pointings were not optimized/adjusted for the fact that the fabricated capsule was about  $145 \mu\text{m}$  larger in radius than the designed capsule. The observed  $^{13}\text{N}$  signal strongly suggests that alpha-particle induced radiochemistry, with its dependence on plasma stopping power, can provide a practical diagnostic for NIF capsule dynamics.



## ACKNOWLEDGMENTS

We thank E. Kemp, Z. Walters, and H. D. Whitley for the design starting point, and J. L. Goodman and P. A. Bradley for insightful discussions. This work was supported by the U.S. Department of Energy through the Los Alamos National Laboratory. Los Alamos National Laboratory is operated by Triad National Security, LLC, for the National Nuclear Security Administration of U.S. Department of Energy (Contract No. 89233218CNA000001).

## DATA AVAILABILITY

The data that support the findings of this study are available from the corresponding author upon reasonable request.

## REFERENCES

- <sup>1</sup>J. Nuckolls, L. Wood, A. Thiessen, and G. Zimmerman, "Laser Compression of Matter to Super-High Densities: Thermonuclear (CTR) Applications," *Nature* **239**, 139 (1972).
- <sup>2</sup>R. S. Craxton, K. S. Anderson, T. R. Boehly, V. N. Goncharov, D. R. Harding, J. P. Knauer, R. L. McCrory, P. W. McKenty, D. D. Meyerhofer, J. F. Myatt, A. J. Schmitt, J. D. Sethian, R. W. Short, S. Skupsky, W. Theobald, W. L. Kruer, K. Tanaka, R. Betti, T. J. B. Collins, J. A. Delettrez, S. X. Hu, J. A. Marozas, A. V. Maximov, D. T. Michel, P. B. Radha, S. P. Regan, T. C. Sangster, W. Seka, A. A. Solodov, J. M. Soures, C. Stoeckl, and J. D. Zuegel, "Direct-drive inertial confinement fusion: A review," *Phys. Plasmas* **22**, 110501 (2015).
- <sup>3</sup>J. Lindl, "Development of the indirect-drive approach to inertial confinement fusion and the target physics basis for ignition and gain," *Phys. Plasmas* **2**, 3933–4024 (1995).
- <sup>4</sup>Lord Rayleigh, "Investigation of the character of the equilibrium of an incompressible heavy fluid of variable density," *Proc. London Math. Soc.* **s1-14**, 170–177 (1882).
- <sup>5</sup>G. I. Taylor, "The instability of liquid surfaces when accelerated in a direction perpendicular to their planes. i," *Proc. R. Soc. London, Ser. A* **201**, 192–196 (1950).
- <sup>6</sup>S. Palaniyappan, J. P. Sauppe, B. J. Tobias, C. F. Kawaguchi, K. A. Flippo, A. B. Zylstra, O. L. Landen, D. Shvarts, E. Malka, S. H. Batha, P. A. Bradley, E. N. Loomis, N. N. Vazirani, L. Kot, D. W. Schmidt, T. H. Day, R. Gonzales, and J. L. Kline, "Hydro-scaling of direct-drive cylindrical implosions at the OMEGA and the National Ignition Facility," *Phys. Plasmas* **27**, 042708 (2020).
- <sup>7</sup>R. D. Richtmyer, "Taylor instability in shock acceleration of compressible fluids," *Commun. Pure Appl. Math.* **13**, 297–319 (1960).
- <sup>8</sup>E. Meshkov, "Instability of the interface of two gases accelerated by a shock wave," *Fluid Dyn.* **4**, 101–104 (1969).
- <sup>9</sup>A. Bose, K. M. Woo, R. Nora, and R. Betti, "Hydrodynamic scaling of the deceleration-phase Rayleigh–Taylor instability," *Phys. Plasmas* **22**, 072702 (2015).
- <sup>10</sup>D. S. Clark, C. R. Weber, J. L. Milovich, J. D. Salmonson, A. L. Kritcher, S. W. Haan, B. A. Hammel, D. E. Hinkel, O. A. Hurricane, O. S. Jones, M. M. Marinak, P. K. Patel, H. F. Robey, S. M. Sepke, and M. J. Edwards, "Three-dimensional simulations of low foot and high foot implosion experiments on the National Ignition Facility," *Phys. Plasmas* **23**, 056302 (2016).
- <sup>11</sup>B. M. Haines, C. H. Aldrich, J. M. Campbell, R. M. Rauenzahn, and C. A. Wingate, "High-resolution modeling of indirectly driven high-convergence layered inertial confinement fusion capsule implosions," *Phys. Plasmas* **24**, 052701 (2017).
- <sup>12</sup>C. R. Weber, D. T. Casey, D. S. Clark, B. A. Hammel, A. MacPhee, J. Milovich, D. Martinez, H. F. Robey, V. A. Smalyuk, M. Stadermann, P. Amendt, S. Bhandarkar, B. Chang, C. Choate, J. Crippen, S. J. Felker, J. E. Field, S. W. Haan, S. Johnson, J. J. Kroll, O. L. Landen, M. Marinak, M. McInnis, A. Nikroo, N. Rice, and S. M. Sepke, "Improving ICF implosion performance with alternative capsule supports," *Phys. Plasmas* **24**, 056302 (2017).
- <sup>13</sup>D. S. Clark, C. R. Weber, J. L. Milovich, A. E. Pak, D. T. Casey, B. A. Hammel, D. D. Ho, O. S. Jones, J. M. Koning, A. L. Kritcher, M. M. Marinak, L. P. Masse, D. H. Munro, M. V. Patel, P. K. Patel, H. F. Robey, C. R. Schroeder, S. M. Sepke, and M. J. Edwards, "Three-dimensional modeling and hydrodynamic scaling of National Ignition Facility implosions," *Phys. Plasmas* **26**, 050601 (2019).
- <sup>14</sup>B. M. Haines, R. E. Olson, W. Sweet, S. A. Yi, A. B. Zylstra, P. A. Bradley, F. Elsner, H. Huang, R. Jimenez, J. L. Kline, C. Kong, G. A. Kyrala, R. J. Leeper, R. Paguio, S. Pajoom, R. R. Peterson, M. Ratledge, and N. Rice, "Robustness to hydrodynamic instabilities in indirectly driven layered capsule implosions," *Phys. Plasmas* **26**, 012707 (2019).
- <sup>15</sup>C. R. Weber, D. S. Clark, A. Pak, N. Alfonso, B. Bachmann, L. F. Berzak Hopkins, T. Bunn, J. Crippen, L. Divol, T. Dittrich, A. L. Kritcher, O. L. Landen, S. Le Pape, A. G. MacPhee, E. Marley, L. P. Masse, J. L. Milovich, A. Nikroo, P. K. Patel, L. A. Pickworth, N. Rice, V. A. Smalyuk, and M. Stadermann, "Mixing in ICF implosions on the National Ignition Facility caused by the fill-tube," *Phys. Plasmas* **27**, 032703 (2020).
- <sup>16</sup>B. Cheng, T. J. T. Kwan, Y. M. Wang, S. A. Yi, S. H. Batha, and F. J. Wysocki, "Effects of preheat and mix on the fuel adiabat of an imploding capsule," *Phys. Plasmas* **23**, 120702 (2016).
- <sup>17</sup>B. Cheng, T. J. T. Kwan, Y. M. Wang, S. A. Yi, S. H. Batha, and F. Wysocki, "Ignition and pusher adiabat," *Plasma Phys. Control. Fusion* **60**, 074011 (2018).
- <sup>18</sup>T. Ma, P. K. Patel, N. Izumi, P. T. Springer, M. H. Key, L. J. Atherton, L. R. Benedetti, D. K. Bradley, D. A. Callahan, P. M. Celliers, C. J. Cerjan, D. S. Clark, E. L. Dewald, S. N. Dixit, T. Döppner, D. H. Edgell, R. Epstein, S. Glenn, G. Grim, S. W. Haan, B. A. Hammel, D. Hicks, W. W. Hsing, O. S. Jones, S. F. Khan, J. D. Kilkenny, J. L. Kline, G. A. Kyrala, O. L. Landen, S. Le Pape, B. J. MacGowan, A. J. Mackinnon, A. G. MacPhee, N. B. Meezan, J. D. Moody, A. Pak, T. Parham, H.-S. Park, J. E. Ralph, S. P. Regan, B. A. Remington, H. F. Robey, J. S. Ross, B. K. Spears, V. Smalyuk, L. J. Suter, R. Tommasini, R. P. Town, S. V. Weber, J. D. Lindl, M. J. Edwards, S. H. Glenzer, and E. I. Moses, "Onset of Hydrodynamic Mix in High-Velocity, Highly Compressed Inertial Confinement Fusion Implosions," *Phys. Rev. Lett.* **111**, 085004 (2013).
- <sup>19</sup>T. Döppner, D. E. Hinkel, L. C. Jarrott, L. Masse, J. E. Ralph, L. R. Benedetti, B. Bachmann, P. M. Celliers, D. T. Casey, L. Divol, J. E. Field, C. Goyon, R. Hatarik, M. Hohenberger, N. Izumi, S. F. Khan, A. L. Kritcher, T. Ma, B. J. MacGowan, M. Millot, J. Milovich, S. Nagel, A. Pak, J. Park, P. Patel, R. Tommasini, P. Volegov, C. Weber, O. L. Landen, D. A. Callahan, O. A. Hurricane, and M. J. Edwards, "Achieving 280 Gbar hot spot pressure in DT-layered CH capsule implosions at the National Ignition Facility," *Phys. Plasmas* **27**, 042701 (2020).
- <sup>20</sup>M. J. Edwards, P. K. Patel, J. D. Lindl, L. J. Atherton, S. H. Glenzer, S. W. Haan, J. D. Kilkenny, O. L. Landen, E. I. Moses, A. Nikroo, R. Petrasso, T. C. Sangster, P. T. Springer, S. Batha, R. Benedetti, L. Bernstein, R. Betti, D. L. Bleuel, T. R. Boehly, D. K. Bradley, J. A. Caggiano, D. A. Callahan, P. M. Celliers, C. J. Cerjan, K. C. Chen, D. S. Clark, G. W. Collins, E. L. Dewald, L. Divol, S. Dixit, T. Doeppner, D. H. Edgell, J. E. Fair, M. Farrell, R. J. Fortner, J. Freije, M. G. Gatu Johnson, E. Giraldez, V. Y. Glebov, G. Grim, B. A. Hammel, A. V. Hamza, D. R. Harding, S. P. Hatchett, N. Hein, H. W. Herrmann, D. Hicks, D. E. Hinkel, M. Hoppe, W. W. Hsing, N. Izumi, B. Jacoby, O. S. Jones, D. Kalantar, R. Kauffman, J. L. Kline, J. P. Knauer, J. A. Koch, B. J. Koziolowski, G. Kyrala, K. N. LaFortune, S. L. Pape, R. J. Leeper, R. Lerche, T. Ma, B. J. MacGowan, A. J. MacKinnon, A. MacPhee, E. R. Mapoles, M. M. Marinak, M. Mauldin, P. W. McKenty, M. Meezan, P. A. Michel, J. Milovich, J. D. Moody, M. Moran, D. H. Munro, C. L. Olson, K. Opachich, A. E. Pak, T. Parham, H.-S. Park, J. E. Ralph, S. P. Regan, B. Remington, H. Rinderknecht, H. F. Robey, M. Rosen, S. Ross, J. D. Salmonson, J. Sater, D. H. Schneider, F. H. Séguin, S. M. Sepke, D. A. Shaughnessy, V. A. Smalyuk, B. K. Spears, C. Stoeckl, W. Stoeffl, L. Suter, C. A. Thomas, R. Tommasini, R. P. Town, S. V. Weber, P. J. Wegner, K. Widman, M. Wilke, D. C. Wilson, C. B. Yeaman, and A. Zylstra, "Progress towards ignition on the National Ignition Facility," *Phys. Plasmas* **20**, 070501 (2013).
- <sup>21</sup>D. S. Montgomery, W. S. Daughton, B. J. Albright, A. N. Simakov, D. C. Wilson, E. S. Dodd, R. C. Kirkpatrick, R. G. Watt, M. A. Gunderson, E. N.

- Loomis, E. C. Merritt, T. Cardenas, P. Amendt, J. L. Milovich, H. F. Robey, R. E. Tipton, and M. D. Rosen, "Design considerations for indirectly driven double shell capsules," *Phys. Plasmas* **25**, 092706 (2018).
- <sup>22</sup>E. L. Dewald, J. E. Pino, R. E. Tipton, J. D. Salmonson, J. Ralph, E. Hartouni, S. F. Khan, R. Hatarik, C. V. Young, D. Thorn, V. A. Smalyuk, R. Sacks, A. Nikroo, N. Rice, S. A. MacLaren, S. Priskrey, B. A. Remington, and F. Graziani, "Pushed single shell implosions for mix and radiation trapping studies using high-Z layers on National Ignition Facility," *Physics of Plasmas* **26**, 072705 (2019).
- <sup>23</sup>J. Colvin, C. Cerjan, R. Hoffman, M. Stoyer, and P. Amendt, "Radiochemical tracers as a mix diagnostic for the ignition double-shell capsule," *Phys. Plasmas* **15**, 102704 (2008).
- <sup>24</sup>D. A. Shaughnessy, C. A. Velsko, D. R. Jedlovec, C. B. Yeamans, K. J. Moody, E. Tereshatov, W. Stoeffl, and A. Riddle, "The Radiochemical Analysis of Gaseous Samples (RAGS) apparatus for nuclear diagnostics at the National Ignition Facility (invited)," *Rev. Sci. Instrum.* **83**, 10D917 (2012).
- <sup>25</sup>Q. Liu, M. Febraro, R. J. deBoer, A. Boeltzig, Y. Chen, C. Cerjan, M. Couder, B. Frentz, J. Görres, E. A. Henry, E. Lamere, K. T. Macon, K. V. Manukyan, L. Morales, P. D. O'Malley, S. D. Pain, W. A. Peters, D. Schneider, C. Seymour, G. Seymour, E. Temanson, R. Toomey, B. Vande Kolk, J. Weaver, and M. Wiescher, "Measurement of the  $^{10}\text{B}(\alpha, n_0)^{13}\text{N}$  cross section for  $2.2 < E_\alpha < 4.9$  MeV and its application as a diagnostic at the National Ignition Facility," *Phys. Rev. C* **100**, 034601 (2019).
- <sup>26</sup>D. C. Wilson, W. Cassata, S. Sepke, C. Velsko, H. Huang, C. Yeamans, J. L. Kline, A. Yi, A. N. Simakov, S. Haan, et al., "Use of 41ar production to measure ablator areal density in nif beryllium implosions," *Phys. Plasmas* **24**, 022701 (2017).
- <sup>27</sup>H. W. Herrmann, N. Hoffman, D. C. Wilson, W. Stoeffl, L. Dauffy, Y. H. Kim, A. McEvoy, C. S. Young, J. M. Mack, C. J. Horsfield, M. Rubery, E. K. Miller, and Z. A. Ali, "Diagnosing inertial confinement fusion gamma ray physics (invited)," *Rev. Sci. Instrum.* **81**, 10D333 (2010).
- <sup>28</sup>N. Otuka, E. Dupont, V. Semkova, B. Pritychenko, A. Blokhin, M. Aikawa, S. Babykina, M. Bossant, G. Chen, S. Dunaeva, R. Forrest, T. Fukahori, N. Furutachi, S. Ganesan, Z. Ge, O. Gritzay, M. Herman, S. Hlavač, K. Katō, B. Lalremruata, Y. Lee, A. Makinaga, K. Matsumoto, M. Mikhaylyukova, G. Pikulina, V. Pronyaev, A. Saxena, O. Schwere, S. Simakov, N. Soppera, R. Suzuki, S. Takács, X. Tao, S. Taova, F. Tárkányi, V. Varlamov, J. Wang, S. Yang, V. Zerkov, and Y. Zhuang, "Towards a More Complete and Accurate Experimental Nuclear Reaction Data Library (EXFOR): International Collaboration Between Nuclear Reaction Data Centres (NRDC)," *Nuclear Data Sheets* **120**, 272–276 (2014).
- <sup>29</sup>S. F. Khan, P. M. Bell, D. K. Bradley, S. R. Burns, J. R. Celeste, L. S. Dauffy, M. J. Eckart, M. A. Gerhard, C. Hagmann, D. I. Headley, J. P. Holder, N. Izumi, M. C. Jones, J. W. Kellogg, H. Y. Khater, J. R. Kimbrough, A. G. Macphee, Y. P. Opachich, N. E. Palmer, R. B. Petre, J. L. Porter, R. T. Shelton, T. L. Thomas, and J. B. Worden, "Measuring x-ray burn history with the Streaked Polar Instrumentation for Diagnosing Energetic Radiation (SPIDER) at the National Ignition Facility (NIF)," in *Target Diagnostics Physics and Engineering for Inertial Confinement Fusion*, Vol. 8505, edited by P. Bell and G. P. Grim, International Society for Optics and Photonics (SPIE, 2012) pp. 33–40.
- <sup>30</sup>V. Y. Glebov, T. C. Sangster, C. Stoeckl, J. P. Knauer, W. Theobald, K. L. Marshall, M. J. Shoup, T. Buczek, M. Cruz, T. Duffy, M. Romanofsky, M. Fox, A. Pruyne, M. J. Moran, R. A. Lerche, J. McNaney, J. D. Kilkenny, M. J. Eckart, D. Schneider, D. Munro, W. Stoeffl, R. Zacharias, J. J. Haslam, T. Clancy, M. Yeoman, D. Warwas, C. J. Horsfield, J.-L. Bourgade, O. Landas, L. Disdier, G. A. Chandler, and R. J. Leeper, "The National Ignition Facility neutron time-of-flight system and its initial performance (invited)," *Rev. Sci. Instrum.* **81**, 10D325 (2010).
- <sup>31</sup>C. L. Ellison, H. D. Whitley, C. R. D. Brown, S. R. Copeland, W. J. Garbett, H. P. Le, M. B. Schneider, Z. B. Walters, H. Chen, J. I. Castor, R. S. Craxton, M. Gatu Johnson, E. M. Garcia, F. R. Graziani, G. E. Kemp, C. M. Krauland, P. W. McKenty, B. Lahmann, J. E. Pino, M. S. Rubery, H. A. Scott, R. Shepherd, and H. Sio, "Development and modeling of a polar-direct-drive exploding pusher platform at the National Ignition Facility," *Phys. Plasmas* **25**, 072710 (2018).
- <sup>32</sup>C. Yeamans, G. Kemp, Z. Walters, H. Whitley, P. McKenty, E. Garcia, Y. Yang, R. Craxton, and B. Blue, "High yield polar direct drive fusion neutron sources at the National Ignition Facility," *Nuclear Fusion* **61**, 046031 (2021).
- <sup>33</sup>F. Ajzenberg-Selove, "Energy levels of light nuclei A=13–15," *Nucl. Phys. A* **523**, 1–196 (1991).
- <sup>34</sup>C. D. Nesaraja and E. A. McCutchan, "ENSDF Full Evaluation," *NDS* **133**, 1 (2016).
- <sup>35</sup>M. Gittings, R. Weaver, M. Clover, T. Betlach, N. Byrne, R. Coker, E. Dendy, R. Hueckstaedt, K. New, W. R. Oakes, D. Ranta, and R. Stefan, "The RAGE radiation-hydrodynamic code," *Comput. Sci. Discovery* **1**, 015005 (2008).
- <sup>36</sup>J. A. Marozas, M. Hohenberger, M. J. Rosenberg, D. Turnbull, T. J. B. Collins, P. B. Radha, P. W. McKenty, J. D. Zuegel, F. J. Marshall, S. P. Regan, T. C. Sangster, W. Seka, E. M. Campbell, V. N. Goncharov, M. W. Bowers, J.-M. G. Di Nicola, G. Erbert, B. J. MacGowan, L. J. Pelz, J. Moody, and S. T. Yang, "Wavelength-detuning cross-beam energy transfer mitigation scheme for direct drive: Modeling and evidence from National Ignition Facility implosions," *Phys. Plasmas* **25**, 056314 (2018).
- <sup>37</sup>B. Haines, D. Keller, J. Marozas, P. McKenty, K. Anderson, T. Collins, W. Dai, M. Hall, S. Jones, M. McKay Jr, R. Rauenzahn, and D. Woods, "Coupling laser physics to radiation-hydrodynamics," *Computers & Fluids* **201**, 104478 (2020).
- <sup>38</sup>N. Meezan, D. Woods, N. Izumi, H. Chen, H. Scott, M. Schneider, D. Liedahl, O. Jones, G. Zimmerman, J. Moody, et al., "Evidence of restricted heat transport in national ignition facility hohlraums," *Phys. Plasmas* **27**, 102704 (2020).
- <sup>39</sup>M. M. Marinak, G. Kerbel, N. Gentile, O. Jones, D. Munro, S. Pollaine, T. Dittrich, and S. Haan, "Three-dimensional HYDRA simulations of national ignition facility targets," *Phys. Plasmas* **8**, 2275–2280 (2001).
- <sup>40</sup>M. J. Schmitt, private communication.
- <sup>41</sup>D. A. Young and E. M. Corey, "A new global equation of state model for hot, dense matter," *Journal of Applied Physics* **78**, 3748–3755 (1995).
- <sup>42</sup>J. Colgan, D. P. Kilcrease, N. Magee, M. E. Sherrill, J. Abdallah Jr, P. Hakel, C. J. Fontes, J. A. Guzik, and K. Mussack, "A new generation of Los Alamos opacity tables," *ApJ* **817**, 116 (2016).
- <sup>43</sup>J. Abdallah Jr and R. E. Clark, "Tops: A multigroup opacity code," Tech. Rep. (Los Alamos National Lab., NM (USA), 1985).
- <sup>44</sup>G. B. Zimmerman, "Recent Developments in Monte Carlo Techniques," (1990), *UCRL-JC-1056016*.
- <sup>45</sup>P. Volegov, S. Batha, D. Fittinghoff, C. Danly, V. Geppert-Kleinrath, C. Wilde, and A. Zylstra, "Three-dimensional reconstruction of neutron, gamma-ray, and x-ray sources using a cylindrical-harmonics expansion," *Rev. Sci. Instrum.* **92**, 033508 (2021).